Nuclear structure in mean-field theory and its extensions

G.F. Bertsch

University of Washingtom

Abstract

This is written for a lecture course given at the 2005 summer school of the Center for Nuclear Study (CNS), University of Tokyo (at the Wako campus of RIKEN).

Contents

PART I: THE STATIC MEAN FIELD

I. INTRODUCTION

A. Self-consistent mean-field theory versus density-functional theory

In virtually all areas of physics, the quantum many-body problem is a computational challenge that still lacks a satisfactory complete solution. Nevertheless, there has been great progress using the concepts of self-consistent mean field theory. I will start my lectures by showing you the progress in condensed matter and quantum chemistry, because the achievements there can serve as an inspiration in nuclear physics, to do better. The fundamental mean field theory in the quantum many-body problem is Hartree-Fock theory, which I will shortly derive. But from a practical point of view it has a limited accuracy, and one can find mean-field theories that are much more accurate without sacrificing the computational advantages of the Hartree theory. I am speaking about density functional theory as formulated by Kohn and Sham in 1966. Let us first look at the numbers and see how these theories perform, and then I'll show you the equations and the particular aspects that are needed for nuclear physics.

From Table I one can see that the simplest form of DFT, called the Local Density Approximation (LDA), is already a factor of two better than Hartree-Fock. But further work on the energy functional gave spectacular improvement, as you can see from the last lines of the table. In this form, the theory became widely used in quantum chemistry.

Although the equations solved have exactly the same form, there is a basic conceptual difference between DFT and SCMF. In DFT, the energy functional has an arbitrary dependence on the ordinary $\rho(r)$ and minimizing the functional is supposed to give the exact ground state of the many-particle system. In SCMF, on the other hand, one starts with

TABLE I: Atomization energies of selected molecules

	Li_2	C_2H_2	20 simple molecules (mean absolute error)
Experimental	1.04 eV	17.6 eV	-
Hartree-Fock [37]	-0.94	-4.9	3.1
LDA [31]	-0.05	2.4	1.4
GGA [38]	-0.2	0.4	0.35
τ [39]	-0.05	-0.2	0.13

a Hamiltonian theory which interaction energy expressible through second quantized operators that depend on density through the combination $\hat{\rho}(r) = a_r^\dagger a_r$. The SCMF is an approximate treatment of the Hamiltonian that can possibly be improved. The mean-field energy may be augmented by additional terms, for example terms that restore the effects of broken symmetry or terms that account for long-range correlations in the wave function.

B. The old and the new in SCMF

Self-consistent mean field theory has a long history in nuclear physics, going back to the pioneering calculations of Brink and his collaborators in the mid 1960's. With the limited computer resources available at the time, one could only treat magic nuclei such as ^{16}O. An important advance was the introduction of the Skyrme parameterization of the energy functional, which effectively decoupled the problem of what the nuclear interaction is, from the problem of describing the structure with some fixed interaction. The Skyrme parameterization simplified the interaction to a contact form. It continues to be used up to the present, but now there are also comprehensive calculations available for SCMF theories with relativistic interactions [7] and with finite-range interactions [8]. Most of the formal development of SCMF and its extensions can be found in the textbook by Ring and Schuck [2]. The present status of SCMF has been reviewed by Bender, Heenen, and Reinhard [1].

II. FUNDAMENTAL EQUATIONS

A. Hartree-Fock and DFT

The fundamental basis of all self-consistent mean-field models is Hartree-Fock theory. Hartree-Fock theory provides a computationally tractable approximation to the general N-particle wave function and can be readily extended as in the Kohn-Sham density functional theory. I shall derive the equations here using second-quantized notation for the HF but ordinary functions for the DFT. I should mention that the second quantized notation is not really needed for the Hartree theory. But the formalism is unavoidable for BCS and the more sophisticated extensions of the theory, and this is a good a place as any to introduce it. The Hartree-Fock approximation approximates the many-particle wave function by the product form

$$|\Phi\rangle = a^\dagger_{k_1} \dots a^\dagger_{k_N} |\rangle.$$

where $a^\dagger_k$ creates a particle in orbital k. In first quantized notation, $|\Phi\rangle$ is the same as the Slater determinant made up of the orbitals k. The relation between the orbital operator and the field operator $\Psi^\dagger$ is $a^\dagger_k = \int d^3r\, \phi_k(r)\Psi^\dagger$, where ϕ_k is the orbital wave function.

In Kohn-Sham DFT one simply takes the orbital wave functions for the occupied orbitals ϕ_k as variational parameters. However, one requires that the orbitals be orthonormal, $\phi^*_k \phi_{k'} d^3r = \delta_{kk'}$.

Consider now a Hamiltonian made of a kinetic energy and a two-body potential

$$H = \int d^3r \frac{\hbar^2}{2m} \nabla\Psi^\dagger(r) \cdot \nabla\Psi(r) + \frac{1}{2}\int d^3r \int d^3r' V(r,r')\Psi^\dagger(r)\Psi^\dagger(r')\Psi(r')\Psi(r).$$

$\Psi(r)$ is the field operator; it creates a nucleon at position r. Using the wave functions $\phi_k(r)$ corresponding to the creation operators $a^\dagger_k$

$$\{\Psi(r), a^\dagger_k\} = \phi_k(r).$$

The expectation value of this Hamiltonian for the Hartree-Fock state Φ is

$$E_\Phi = \langle\Phi|H|\Phi\rangle = \sum_i^N \frac{\hbar^2}{2m}\int d^3r \nabla\phi^*_k(r)\cdot\nabla\phi_k(r) + \sum_{a<b}\int d^3r \int d^3r' V(r,r')|\phi_a(r)|^2|\phi_b(r)|^2 \quad (1)$$

$$-\sum_{a<b}\int d^3r \int d^3r' V(r,r')\phi_a{}^*(r)\phi_a(r')\phi_b{}^*(r')\phi_b(r).$$

The first potential energy term above is the *direct* or *Hartree* energy and the second is the *exchange* or *Fock* energy.

The corresponding expression in DFT is the energy function, defined in terms of the orbitals ϕ_k and the particle density $\rho(r) = \sum_k |\phi_k(r)|^2$ as

$$\int d^3r \left(\sum_k \frac{|\nabla \phi_k|^2}{2m} + \mathcal{V}(\rho(r)) \right)$$

We find the optimum orbitals by minimizing this expression. At the minimum, the variation with respect to the form of the orbitals vanishes. This is expressed by the variational equations

$$\frac{\delta}{\delta {\phi_k}^*(r)} (\langle \Phi | H | \Phi \rangle - \sum_{ij} \lambda_{ij} \langle \phi_i | \phi_j \rangle) = 0.$$

The λ_{ij} are Lagrange multipliers that enforce the orthonormality of the single-particle states.

Defining the density matrix, $\rho(r, r') = \sum_i^N |\phi_i(r)|^2$, the Hartree potential $V_H(r) = \int d^3r' V(r, r') \rho(r', r')$, and the Fock potential $V_F(r, r') = V(r, r') \rho(r, r')$, a single-particle Hamiltonian can be defined

$$(h\phi_k)(r) = -\frac{\nabla^2}{2m} \phi_k(r) + V_H(r) \phi_k(r) - \int d^3r' V_F(r, r') \phi_k(r').$$

Using this definition, the Hartree-Fock equations can be written

$$h\phi_k(r) = \sum_i^N \lambda_{ki} \phi_i(r).$$

The right-hand side can be further simplified by solving for the Lagrange multipliers

$$\lambda_{ki} = \langle \phi_i | h | \phi_k \rangle.$$

Because $h = h^\dagger$, the matrix λ composed of the λ_{ki} is Hermitian, and can be diagonalized with a unitary transformation S. Defining $\psi = S\phi$, where ϕ is composed of the elements ϕ_i, the Hartree-Fock equations simplify to

$$h\psi_i = \epsilon_i \psi_i \tag{2}$$

where the ϵ_i are the eigenvalues of λ. We shall see in Sect. III how one can efficiently solve this system of N coupled differential equations.

B. HF-BCS

A very important generalization of the Hartree-Fock theory is to pairing theory. It may viewed as a mean-field theory includes both particle creation and annihilation operators in the definition of the mean-field orbitals. The general equations governing the orbitals are the Hartree-Fock-Bogoliubov equations, called the Bogoliubov-deGenne equations in condensed matter physics. I will present the equations in the next subsection; here I will present the simpler BCS theory [3]. In the BCS theory as carried out in nuclear physics, we first solve the HF equations to get a set of orbitals k. In favorable cases such as in dealing with even-even nuclei, the HF equations are invariant under time reversal. This implies that each orbital k has its time-reversed parter $\bar{k}$, and the two have the same single-particle energy ϵ_k. Now we come to the basic BCS Ansatz, to take the many-particle wave function to have the form

$$|\mathrm{BCS}\rangle = \prod_{k>0} (u_k + v_k a_k^\dagger a_{\bar{k}}^\dagger)|\rangle.$$

The u_k and v_k are parameters are to be determined by minimizing the expectation value of the Hamiltonian. Normalization of the state requires

$$|u_k|^2 + |v_k|^2 = 1.$$

The BCS state is not an eigenstate of the particle number operator. However, by augmenting the Hamiltonian with a Lagrange multiplier term,

$$H \to H - \lambda \hat{N},$$

the particle number expectation value can at least be fixed to the desired value N,

$$\langle BCS|\hat{N}|BCS\rangle = 2\sum_{k>0} v_k^2 = N.$$

I now give two examples of BCS pairing that shows the range of pairing effects in nuclei. The first is a Hamiltonian with degenerate orbitals and a constant pairing interaction. Let us suppose there are 2Ω orbitals including the time-reversed partners and N_p particles (either neutrons or protons). First consider an even number of particles. Then the v_k amplitudes are all equal and are determined by fixing the number of particles to N_p. Namely,

$$v_k^2 = \frac{N_p}{2\Omega}.$$

There is no single-particle energy in the Hamiltonian so its expection value is just that of the interaction. Let us take it to be $-g$ for all orbitals. Then we have

$$\langle BCS|v|BCS\rangle = -\frac{1}{2}\sum_{k}^{\Omega}\sum_{k'}^{\Omega}\frac{N_p}{2\Omega}\left(1-\frac{N_p}{2\Omega}\right)$$

$$= -\frac{g}{8}N_p(2\Omega - N_p). \text{ (even)}$$

If there are an odd number of particles, one will be alone in some particular orbital blocking the parter orbital. Thus the pairing will now occur among the $N_p - 1$ remaining particles occupying the $\Omega - 1$ available orbitals. Thus the energy in this case is

$$\langle BCS|v|BCS\rangle = \frac{g}{8}(N_p - 1)(2\Omega - N_p - 1) \text{ (odd)}.$$

If you try out these formulas with not too small a value for Ω, you will see that the even systems have lower energies that the average of the neighboring odd systems. The precise amount of this pairing varies, but with the orbitals half filled it is about $g\Omega/4$.

Another simple model is called the picket fence Hamiltonian. The orbitals (together with their degenerate time-reversed partners have an equal energy spacing. Let's call the spacing ϵ_0. Again we assume that the interaction has equal matrix elements for all the orbitals. In this case, we need to impose a cutoff on the single-particle spectrum to get a solution of the BCS equations. Let us suppose that the cutoff is the same above and below the Fermi energy, and that it is large compared to ϵ. If the pairing strength is such that Δ comes out large compared to ϵ_0 but small compare to the cutoff energy, the total energy (compared to that of the same system without the pairing interaction is given by

$$E = -\frac{\Delta^2}{2\epsilon_0},$$

and the difference in energy between even and nearby odd systems is

$$E_{odd} - E_{even} = \Delta.$$

C. HFB

In the last section, the variation to find the pairing amplitudes u_k, v_k was performed after the HF variation to set the orbitals k. Can one do better doing both variations at the same time? The answer is yes, at least in principle. An elegant formulation of the problem is given

by the HFB equations. It is easiest to think about these equations in a finite-dimensional basis of orbitals, say with dimension M. In that basis, the Hartree-Fock Hamiltonian h is an $M \times M$ matrix. We only need the lowest N eigenvectors of the matrix to get the density and the occupied orbitals. In contrast, the HFB matrix has twice the dimension, $2M \times 2M$, and all the eigenvectors are needed in principle to find the densities. For details of equations see the book by Ring and Schuck [2].

The question remains whether the HFB is necessary for reliable theory. When active orbitals are well bound as in ordinary nuclei along the valley of stability, the orbitals do not change appreciably from the pairing field and the ordinary BCS treatment is entirely adequate. This may not be the case for drip-line nuclei, where the pairing could make the difference between bound and unbound orbitals. However, in a recent work, Hagino and Sagawa showed that even under dripline conditions the effects of the HFB could be obtained by a simple perturbative treatment of the BCS wave function [46].

III. COMPUTER PROGRAMS

A. Choice of basis

Two leading choices are a coordinate-space mesh and harmonic oscillator wave functions[1].

The 3-D coordinate space mesh was introduced to mean-field calculations in nuclear physics in 1978 to solve the equations of time-dependent mean-field theory [9]. The method was then applied to the static problem, and a state-of-the-art computer program `ev8.f` is now available for anyone to use [4]. The other method, expansion in harmonic oscillator function, is also available in a distributed program [6]. I am more familiar with the `ev8.f` program, so we will use that one for the examples.

With a coordinate mesh, there will be two numerical parameters to be specified, the mesh spacing Δx and the number of mesh points N_r. In `ev8.f` the mesh fills a rectangular box. The sides are usually taken to be equal so the number of mesh points is $N_r = N_x^3$. It is

[1] This contrasts with quantum chemistry and condensed matter. In quantum chemistry, the leading choice is a basis of Gaussian functions, while in condensed matter a mesh in momentum space is popular. It should mentioned that from a computational point of view, meshes in coordinate or in momentum space are not so different because one can easily transform from one basis to the other by the fast Fourier transform.

assumed that all the orbitals have a reflection symmetry with respect to the three coordinate axes; this allows the meshed space to be one eighth of the total. Thus, the length of a side of the box is $L_x = 2N_x\Delta x$. We shall go through an example below for the nucleus ^{48}Ca, for which the parameters have values $\Delta x = 0.8$ fm and $N_x = 14$. Thus the distance from the center of the nuclei to a wall of the box is 11.4 fm. This should be compared with the nominal radius of the nucleus, $R = 1.2A^{1/3} = 4.4$ fm. The size of a real vector needed to represent an orbital is the number of mesh points times two for the two spin states times an additional factor of two for the real and imaginary parts of a complex amplitude. Thus for the ^{48}Ca example, the vector size is $14^3 \times 4 \approx 11,000$.

An important property of the mesh representation is that the single-particle Hamiltonian is a sparse matrix. The kinetic energy operator may be approximated by difference formulae that only involve nearby mesh points. Or, if one wants to treat the kinetic energy more exactly and is willing to accept periodic boundary conditions on the lattice, one can use the Fast Fourier Transform. That derives its speed from a sparse matrix representation. Concerning the potential energy, due to the short range of the nuclear interaction it only requires amplitudes on nearby mesh points as well.

In the harmonic oscillator representation, the important numerical parameters are the oscillator frequencies $\omega_x, \omega_y, \omega_z$ and the number of oscillator states included. Usually, there is a maximum for number of oscillator quanta N, where $N = n_x + n_y + n_z$.

B. Method of solution

Given the single-particle Hamiltonian in some representation, one can solve for the orbitals in eq. (2) by direct diagonalization if the dimensions are not too large. This is the case for the harmonic oscillator representation, but not for the lattice representation. In the latter case, one uses iterative techniques. They all have in common that the solution is built out of repeated applications of the Hamiltonian matrix to a vector. These matrix-on-vector operations are at the heart of the well-known Lanczos method of matrix diagonalization. However, for the problem at hand, many eigenfunctions are needed–one for each occupied orbital–and other methods are more robust. A common method is to (approximately) exponentiate the single-particle Hamiltonian to filter the ground orbital out of mixed wave

function,

$$\phi_f = \exp(-\beta h_0)\phi_i$$

The component of an eigenstate k with energy ϵ_k is suppressed by a factorexp$(-\beta\epsilon_k)$ which is relatively larger the higher the energy of the component. When this procedure is used, one starts with a crude approximation to the N_p distinct orbitals. At each stage of the filtering, the orbitals are orthonormalized by the Gram-Schmidt procedure. The numerical parameters here are β and the number of iterations M_β needed for the desired accuracy.

The self-consistency of the SCMF is achieved by iterating over solutions of the single-particle Hamiltonian, updating it by the improved information about the densities at each stage. To make the procedure stable and convergent, one usually updates by the replacement $\rho_{old} \rightarrow \alpha\rho_{new} + (1-\alpha)\rho_{old}$ where α is a numerical parameter. A final numerical parameter is the number of HF iterations M_{HF} needed for satisfactory convergence.

C. An example: ^{48}Ca

In this section, we will go through a specific example, just to see how `ev8` works from a user's perspective. First, log on to the computer, make a directory for yourself, and run the program using a script to do all the work. The actual steps from a terminal window are:

```
ssh riken@gene.phys.washington.edu
password:  ev8.f
mkdir <your name>
cp -r ev8 <your name>
cd <your name>
example.sh
```

If all goes well, you will see the program compiling and then running with the output to the screen. The last the lines will be:

```
********** Ecm v2 **************
* neutron =        6.215248 MeV *
*  proton =        3.303791 MeV *
*   total =        9.519039 MeV *
*********************************

 ***** THE END *****
```

Let's look at the input file that was constructed to run this case. It is called `data`, and it reads:

```
ev8
    0     0     0
 0.99999998E-02
  -25     0     0
   10     0     0     0
   28    20
Sly4
    5     1     0     0
 0.10000000E+04 0.50000000E+01 0.00000000E+00 0.16000000E+00
 0.10000000E+04 0.50000000E+01 0.00000000E+00 0.00000000E+00
    1     1
 0.10000000E+00 0.20000000E-01 0.40000000E+04
 0.00000000E+00 0.00000000E+00
 0.00000000E+00 0.10000000E+05
 0.75000000E-02 0.00000000E+00
```

I will only explain the entries that need to be changed for later tests. The first is the "-25" on line 4, which instructs the program to make 25 HF iterations. The second is the "5" on line 8, which specifies the Lipkin-Nogami treatment of pairing. Let us change the "5" to a "4", specifying the BCS treatment of pairing, and run the program again with the command line: `|>ev8.exe < data > 028.020.out` Now we have the output in the file `028.020.out` and can examine it at leisure. Just below the header one can see the lines

```
 mass =   48  charge =   20  n =   28

 nx=   16            ny=   16            nz=   16
 dx= 0.80000000E+00Fm
```

This tell us that the input wave function file was describing the nucleus ^{48}Ca, using lattice parameters $N_x = N_y = N_z = 16$ and a mesh spacing of $\Delta x = 0.8$ fm, as remarked in a previous section. Let us now jump down and find the section where it reports the properties of the neutron orbitals:

```
 neutron levels
   n  par  vbcs    vln     del     eqp     esp       jz    d2(h)
   1    1   1.000   1.000   0.193  41.733 -49.838   0.500 -9.25E-07
  17   -1   1.000   1.000   0.521  28.085 -36.191   0.500 -1.02E-04
  18   -1   1.000   1.000   0.522  28.052 -36.157  -1.500 -7.42E-07
  19   -1   1.000   1.000   0.477  24.992 -33.097   0.500 -1.02E-04
   2    1   1.000   1.000   0.874  14.543 -22.649   0.500 -4.06E-05
   3    1   1.000   1.000   0.876  14.516 -22.621  -1.498 -3.52E-05
   4    1   1.000   1.000   0.874  14.493 -22.598   2.497  2.31E-05
   5    1   1.000   1.000   0.888   9.599 -17.704   0.500 -2.96E-03
   6    1   1.000   1.000   0.836   8.304 -16.409   0.500 -2.96E-03
   7    1   1.000   1.000   0.836   8.254 -16.359  -1.498 -3.48E-05
  20   -1   0.929   0.963   1.125   2.183  -9.848   0.499 -1.22E-04
  21   -1   0.928   0.962   1.126   2.171  -9.832  -1.498 -4.91E-05
  22   -1   0.927   0.961   1.126   2.153  -9.808   2.497 -2.04E-05
  23   -1   0.926   0.961   1.123   2.137  -9.790  -3.494 -5.10E-05
  24   -1   0.135   0.074   0.840   1.230  -5.610   0.499 -3.18E-04
  25   -1   0.129   0.069   0.837   1.247  -5.572  -1.498 -7.25E-05
```

The first line of numbers tells us properties of orbital no. 1. The most basic properties are in columns 2,3,7 and 8. They are:

TABLE II: Binding energy of ^{48}Ca.

Source	Binding Energy
SLy4 [10]	417.87
`hfbtho`	417.84
`ev8`	418.48
exp.	415.99

- parity, 1 (even);
- occupation probability, $v_1^2 = 1.000$;
- single-particle energy, $\epsilon_1 = -49.838$ MeV;
- angular momentum, $j_z = 0.500$.

Obviously, this is the $0s_{1/2}$-orbital. Now, can you find some of the other shell orbitals? The nucleus is spherical, so there should be a energy degeneracy for different j_z-states for a given j. Note that only one of the orbitals in a k,$\bar{k}$ is listed, and that the j_z of the listed orbital can be either positive or negative. ^{48}Ca is supposed to be a magic nucleus. One characteristic is a gap in the single-particle levels between occupied and unoccupied levels. Verify that the proton gap is between the $f_{7/2}$ and the $d_{3/2}$ shells with a value of 5.7 MeV, and the neutron gap is between the $f_{7/2}$ and the $p_{3/2}$ shells with a value of 4.3 MeV.

Finally, the total energy of the nucleus is given toward the bottom of the output file, in the line

```
total energy (from functional) -418.480 energy per nucleon 8.718
```

We compare this value with ones obtained from other sources in Table II.

At this point I should say something about the energy functional underlying the calculation. It was done with the "SLy4" parameterization [10] of the Skyrme energy functional, and in fact the binding energy of this nuclei was one of properties considering in constructing it. Their number, obtained with a spherical code, is shown on the top row. The code `hfbtho` is also quite accurate although it is a 3-dimensional code. We can see that these number agree for the purposes on nuclear mass tables (several hundred KeV). While program `ev8.f` is somewhat less accurate, for other properties such as single-particle spectra and separation

TABLE III: . Energy of the $f_{7/2}$ neutron orbital in ^{48}Ca by various methods. All energies are in MeV.

Source	$\epsilon(f_{7/2})$	(E(^{48}Ca)-E(^{46}Ca))/2
`ev8`	-9.8	-8.15
`hfbtho`	-9.8	-8.5
Exp.		-8.6

energies the results are virtually identical to other code outputs. The theory misses the experimental value by 2 MeV, which is rather typical.

IV. ELEMENTARY APPLICATIONS

Let us first examine the orbital energies of the SCMF, taking the example of ^{48}Ca.

A. Separation energies

The neutron and proton separation energies are defined by the difference in binding energies

$$S_n = E(N,Z) - E(N-1,Z)\,; \;\; S_p = E(N,Z) - E(N,Z-1)$$

Naively, we might identify the orbital energies ϵ_k as separation energies, but that is only an approximation based on the assumption that the other occupied orbitals remain the same when a nucleon is removed from the nucleus. More rigorously, the separation energy should be calculated by taking energy differences between the nuclei with and without that particle. The two methods are compared in Table III. Note that the difference energy is more accurate than the orbital value. This is due to changes in the wave function such as a pairing-nopairing transition from one nucleus to the other. These contributions, called rearrangement energies, are not included in the ϵ_j. Still, the naive identification has some value as the orbital rearrangement effects are not large. This is not the case for electronic systems. There the orbital energies can be quite misleading.

TABLE IV: Neutron particle states in ^{49}Ca.

Shell	$\epsilon_j - \epsilon_{3/2}$	Experimental
$p_{3/2}$	0.0	g.s.
$p_{1/2}$	1.9	2.0
$f_{5/2}$	4.2	~ 4.0

TABLE V: Proton hole states in ^{47}K.

Shell	$\epsilon_j - \epsilon_{1/2}$	Experimental
$s_{1/2}$		g.s.
$d_{3/2}$		0.4
$d_{5/2}$		~ 5.0

B. Particle orbitals

The orbital energy differences among the unoccupied (particle) orbitals should be reflected in the spectrum of the nucleus with one added particle, which may be placed in any of the unoccupied orbitals. Because we only consider energy differences, rearrangement effects should be reduced. The same reasoning can be made for the occupied (hole) orbitals as well, giving predictions for the spectrum of the nucleus with one less particle. Table IV shows the comparison for the ^{48}Caneutron particle orbitals. The results look very nice, but the situation is in fact more complicated. In the experimental spectrum of ^{39}Ca, the $p_{1/2}$ can be easily identified, being with the first excited state and well isolated in the spectrum. However, the higher spectrum has many states below 4 MeV, and the $f_{5/2}$ is only identified by reaction properties (namely, the (d,p) reaction). Finally, in Fig. 1 we show graphs of the single-particle orbitals of various light- and medium-weight nuclei. The experimental numbers were from the separation energies with respect to neighboring odd nuclei. **Exercise:** use the output of ^{48}Ca calculation to fill in the entries in Table V.

C. Particle-hole gaps

The last orbital energy comparison we make is for the particle-hole shell gap, already extracted for ^{48}Ca in Sect. III C. In a naive shell model, this energy should reflect a gap

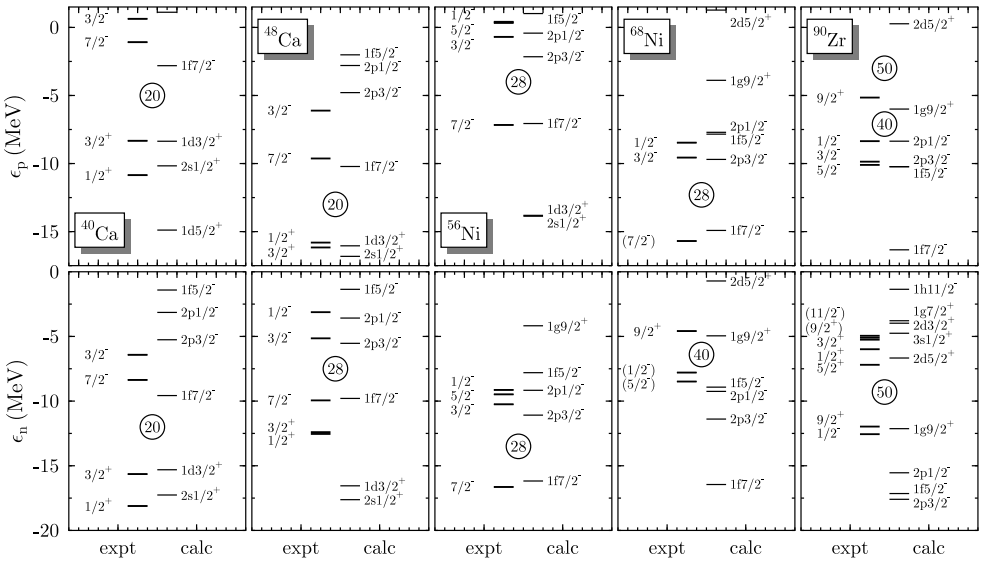

FIG. 1: Spectra of light- and medium-mass doubly magic nuclei, calculated in the SCMF with the SLy4 energy functional.

in the excitation spectrum. Experimentally, the first excited state of ^{48}Ca is a $J = 2$ even parity state (2^+) at excitation energy of 3.8 MeV. The state could not come from the proton shell gap, because the parities of the particle and hole states are different. It could come from the neutrons, however, exciting an $f_{7/2}$ neutron to the $p_{3/2}$ shell. The angular momentum of the state can be anywhere in the range of $|j_p - j_h|$ to $j_p + j_h$, so the quantum number 2^+ is permitted. The orbital gap energy is 4.3 MeV, somewhat larger than the observed value. In fact, effects of the residual interaction and of wave function mixing will be strong in such cases, so the naive energy should only be considered qualitative at best. We will consider the excitations in much more detail when we come to the extensions of SCMF.

D. Shell closures

Much experimental research has been directed to finding new shell effects in nuclei far from stability. With the SCMF and computer resources one now has available, theorists can see if there is an overall global consistency and provide predictions any region of the mass table. The main signatures of shell closures are:

Binding energies. Shell effects can be seen in the trends of nuclear binding energies when the smooth parts of the binding are subtracted out. This is shown very graphically in

the plot of residuals with respect to the liquid model [13]. A version of that plot with experimental data from the latest compilation [17] is Fig. 2. The residuals are plotted as a function of neutron number, with data for the same proton number connected by lines. The shell closures at $N = 50, 82,$ and 126 are very prominent. There are no obviously binding effects of shell closures in light nuclei.

Two-nucleon gap A more sensitive measure of shell effects comes from differences in binding energies. The two-nucleon separation energy is less sensitive to pairing effects than the ordinary separation. It is given by

$$S_{2n} = E(N, Z) - E(N - 2, Z)$$

for the case of neutrons. The separation energy should be larger at a magic number than above the magic number, because the nucleons come from different shells. Thus the energy difference

$$\delta_{2n}(N, Z) = S_{2n}(N + 2, Z) - S_{2n}(N, Z)$$

should be an measure of the shell closure. It is called the *two-nucleon gap*.

As an exercise, let us find the nuclei with largest values of $\delta_{2n}(N, Z)$ and see what shells they mark. Because the shell spacing are larger for smaller nuclei, we should make a criterion that scales with nuclei size according to the single-particle level spacing. Let us make the criterion be

$$\delta_{2n}(N, Z) > \frac{16}{A^(1/3} \text{ MeV}$$

Experimentally, there are 30 nuclei that satisfy this criterion. Their characteristics are shown in Table VI. One sees very clearly the magic numbers 28,50,82 and 126. The other even-even nuclei that have large gaps turn out to be lighter nuclei on the $N = Z$ line. There is thus an enhanced stability of the so-called "alpha-particle nuclei". The predictions of SCMF with SLy4 are qualitatively similar but not identical. There are more magic nuclei and relatively fewer alpha-particle nuclei passing its two-neutron gap test. From the table, one sees that $N = 20$ qualifies as a magic number in the SCMF but not experimentally.

Excited state gap. The most sensitive measure of shell effects is the systematic trend of the energy gap in the excitation spectra. The first excited state of most even-even

TABLE VI: Even-even nuclei with large two-neutron gaps

$N = Z$?	N	Exp.	SLy4
yes		12	4
no	N=20	0	3
	28	2	3
	50	5	5
	82	7	7
	126	4	5
	other	0	2
total		30	29

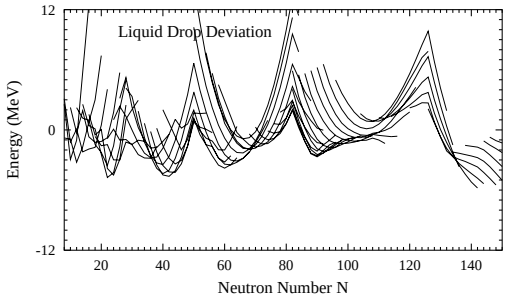

FIG. 2: Binding energy residuals for the liquid drop model (after [13]).

nuclei has quantum number 2^+, and its excitation energy becomes large in a magic nucleus. The systematics of the 2^+ excitation energies is shown in Fig. 3, plotted as a function of proton number. The very large values (> 3.5MeV) are associated with doubly magic nuclei, ^{40}Ca, ^{132}Sn and ^{208}Pb. Note that in the $N = 82$ chain there is an apparent minor shell closure at $Z = 64$.

E. Deformations

Alongside the explanation of magic numbers and shell closures, a great success of the SCMF is its description of deformed nuclei. Let us take as an example the nucleus ^{162}Dy. If we put in its particle numbers $N = 96$, $Z = 66$ in the code `ev8` we find that the SCFM is not spherical. To see this, run the code and find a line with the notation 'qtot'. It gives the expectation value of the quadrupole operator $Q = 2z^2 - x^2 - y^2$. The converged value

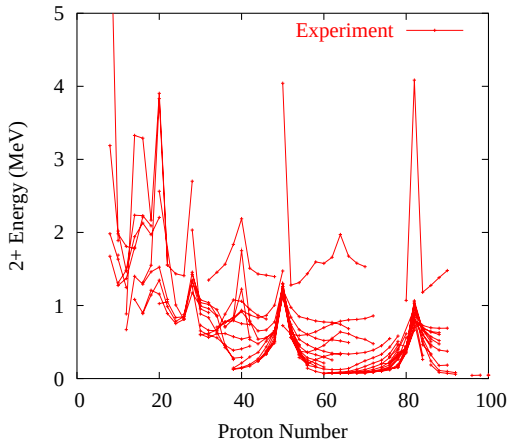

FIG. 3: Systematics of 2^+ excitation energies.

for ^{162}Dy is $Q_0 \sim 1800$ fm^2

What is the physical meaning of this number? The ground state of ^{162}Dy as angular momentum zero and thus no quadrupole moment. But in an important sense it is indeed physical, describing a the intrinsic state of the ground state rotational band. Thus to compare with experiment one has to examine band properties. The easiest one to use is the reduced quadrupole transition rate $B(E2)$ connecting the excited 2^+ state in the band to the 0+ ground state. A simple formula can be derived in the rigid rotor model to relate it to Q_p, the intrinsic quadrupole moment of the proton distribution in the intrinsic state. The formula is [18, eq. 4-68b]:

$$B(E2; 0 \to 2) = \frac{5e^2}{16\pi} Q_p^2 \approx \frac{Z^2 e^2}{16\pi A^2} Q_0^2$$

. We can get the experimental value from the compilation by Raman et al. [22], $B(E2; 0 \to 2) = 5.3$ e^{2}bn^2. The deduced value of Q_p and Q_0 are then 7.3 bn and 17.8 bn respectively. The agreement between theory and experiment is perfect within the accuracies of the experimental measurement and the numerical calculation. We can't expect to do so well in general. It is common to express the deformation in terms of the shape parameter β_2. Although in principle β_2 has a geometric definition, in practice it is often defined by the formula

$$Q_0 = \frac{1}{\sqrt{5\pi}} \beta_2 A^{5/3}\, 1.44\, \mathrm{fm}^2.$$

With this definition, $\beta_2 = 0.34$ for ^{162}Dy.

The importance of deformation in the SCMF energies is illustrated in Fig. 4, showing

FIG. 4:

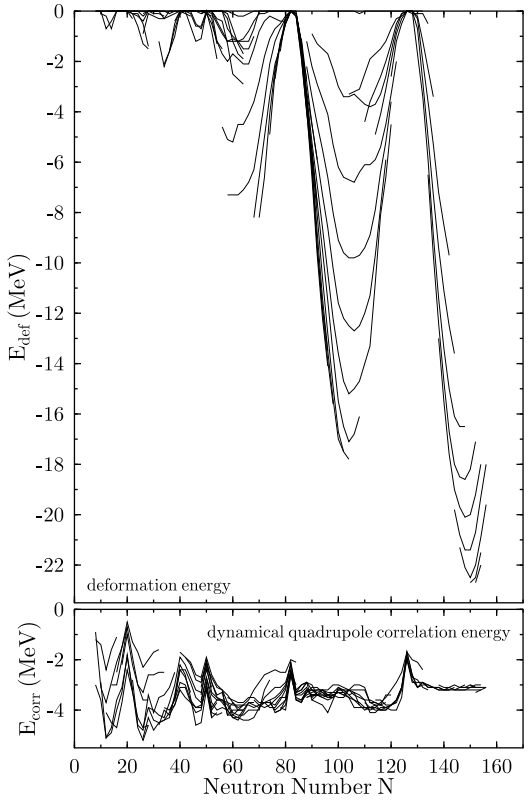

the energy differences between the SCMF with and without breaking spherical symmetry. We see that the deformation can contribution up to 20 MeV in the total energy.

F. Binding and separation energy systematics

Computer resources are now adequate to perform the SCMF calculations for all nuclei of interest at once, even varying the parameters of the energy functionals. Thus, it is now possible to construct theoretical mass tables using SCMF. We can then begin to duplicate the program of quantum chemistry where the DFT was improved to the point of being useful to predict the properties of unknown systems. The first mass theory was the liquid drop model, whose predictions were shown in Fig. 2. The rms residual of theoretical and experimental binding energies is about 3 MeV. A theory including shell effects that has become the benchmark for binding energies is the finite-range droplet model (FRDM) of Möller et al. [13]. It has between 10 and 20 adjustable parameters, achieving a fit to the known masses having an rms residual of about 600-700 keV. A guiding principle in that theory was to try to simulate SCMF to correct the liquid drop formula for shell effects.

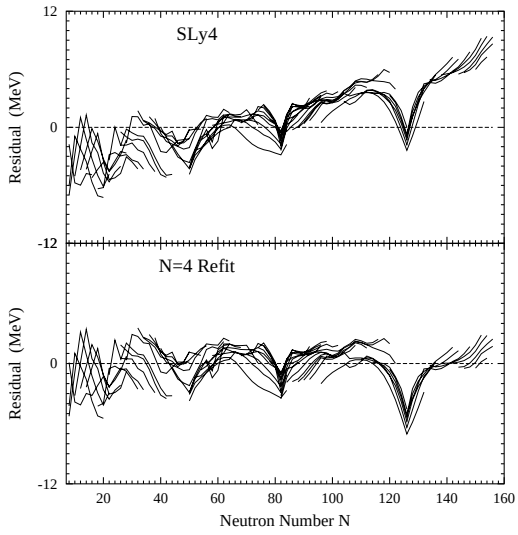

FIG. 5: Binding energy residuals of the SCMF theory using the refitted SLy4 parameter set [14].

However, it turns out that "true" SCMF does not come close to the accuracy of the FRDM, at least with the Skyrme parameterization framework. Ref. [14] shows that the accuracy is limited to about 1.5 MeV using Skyrme parameterizations. A plot of residuals is shown in Fig. 5 One sees that the SCMF overemphasizes the shell stability at neutron magic numbers $N = 50, 82, 126$. The Skyrme SCMF was also used by Goriely, et al., [19] to construct a mass table. These authors included additional phenomenological terms in theory and were then able to achieve fits comparable to the FRDM.

There is an interesting shell effect visible in the systematics of the two-nucleon gaps, called "mutually enhanced magicity". One finds that the gaps are largest when both protons and neutrons are at magic numbers. Thus, there is an interaction between the protons and neutrons that can either enhance or diminish shell effects. This behavior is illustrated in Fig. 6, showing the two-proton gaps at $Z = 50$ and 82 as function of neutron number. The observed gaps, shown by diamonds, peak at $N = 82$ in the Sn isotopes and at $N = 128$ in the Pb isotopes. In contrast, the SCMF restricted to spherically symmetric fields has a flat behaviors, shown by the short-dashed lines. Allowing static deformations reduces the

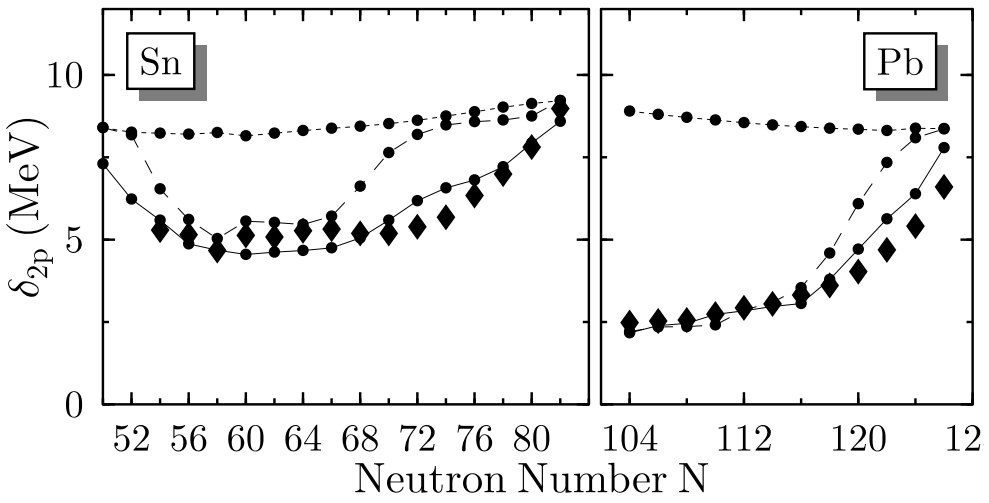

FIG. 6: Two-proton gaps for Pb and Sn isotopic chains. Observed gaps are shown by diamonds.

gap in the mid-shell region, as seen by the long-dashed curve. However, it does nothing near the magic numbers where the nucleus remains spherical. We will get to the theory corresponding to the solid line later.

I would like to tell you a bit how we did the fit because it is a common problem and many people waste a lot of time discovering the pitfalls for themselves. We represent the energy functional as a sum of terms

$$\mathcal{V} = \sum_{i=1}^{10} c_i f_i$$

where c_i is a parameter and f_i is a function of the one-body densities.The interaction energy for each nucleus A requires the integrals over the corresponding densities f_{iA},

$$I_{iA} = \int d^3r f_{iA}.$$

Then the theoretical energy for each nucleus is

$$E_{th}(A) = \sum_{i=1}^{10} c_i I_{iA}$$

and the errors, called *residuals*, is given by

$$r_A = E_{exp}(A) - E_{th}(A).$$

One can do a linear refit just using this information. According to the Feynman-Hellman theorem [32], the derivative of the residuals with respect to the parameters is given by

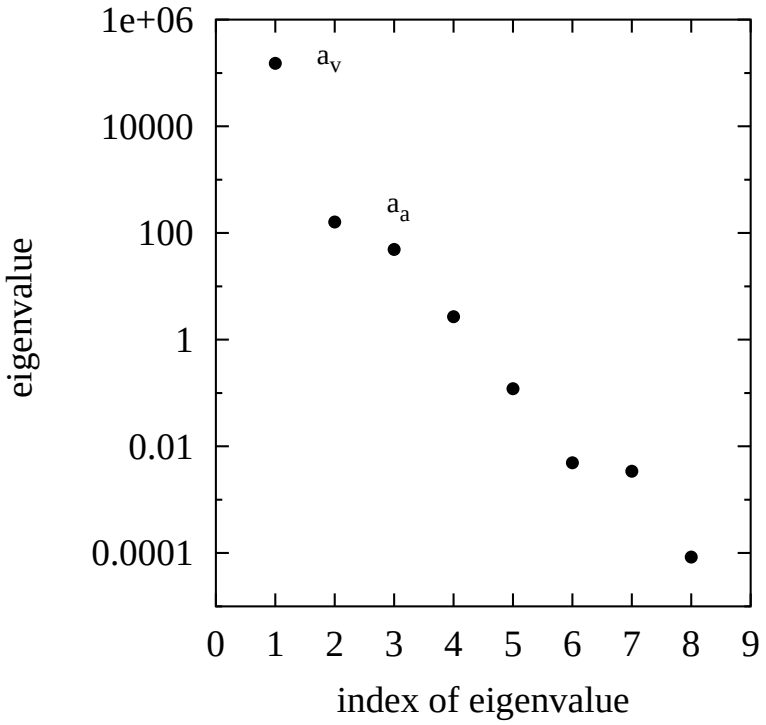

FIG. 7: Eigenvalues of the least square fitting matrix M. .

$dr_A/dc_i = I_{iA}$. The linear least squares fit requires inverting the matrix M having elements

$$M_{ij} = (II^\dagger)_{ij} \equiv \sum_A I_{iA} I_{jA}. \tag{3}$$

The refit parameters are changed by an amount Δc given by

$$\Delta c = M^{-1} I^\dagger r.$$

Here Δc and r are vectors with components c_i and r_A respectively.

The problem that often arises when using this formula is that the matrix M can be singular, and thus not invertible. This happens when there are redundant combinations of parameters, or parameters that are very insensitive. The remedy is to first diagonalize M and project onto a smaller space that eliminates the small eigenvalues.

Fig. 7 shows the eigenvalue spectrum for the M matrix derived from the residuals of the ~ 550 known even-even nuclei [14]. The eigenvalues have a remarkable span of values. We can also see which combinations of parameters determine the nuclear matter binding energy a_v and the symmetry energy a_s. It turns out that these combinations are essentially contained in the subspace of the first three vectors, with the first vector determining a_v. The

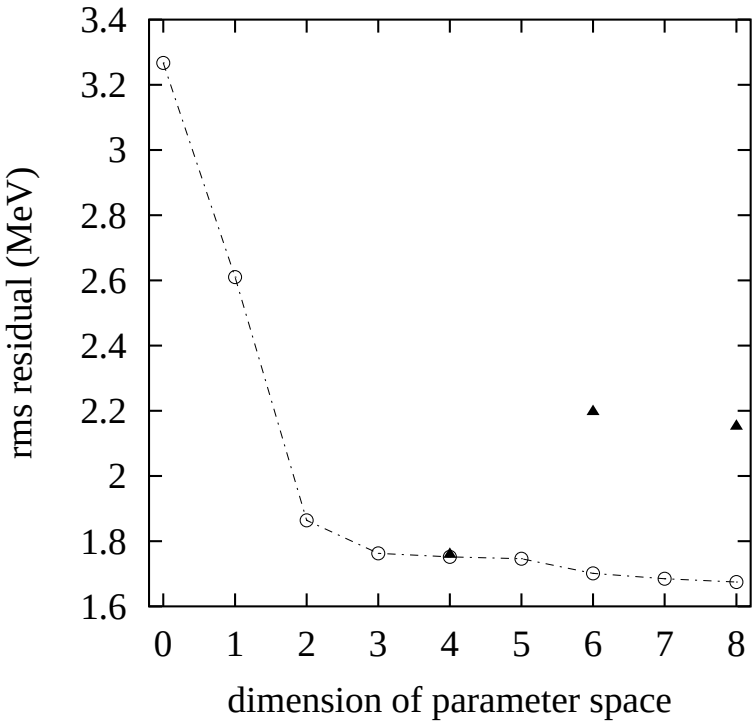

FIG. 8: RMS residuals of refitted binding energies.

next figure shows how the rms residual of the binding energies improve as one augments the fitting space. Essentially, one only needs the information from the first four vectors to fit the binding energies. This is confirmed by doing a full refit, which gives the same result with four-dimensional fit but a larger error for six or eight dimensions.

Another fitting procedure we have tried is the minimax method [14]. It gives a table of critical nuclei, the nuclei that are most difficult to fit. It can be more sensitive to new data than the traditional least squares fit. This is illustrated in Table VII, making fits with the liquid drop model. The first two lines are fits to the data in the 2003 and the 1995 mass tables. Paradoxically, the r.m.s. residual improves with time but the minimax norm gets worse. When we looked closer at the new data, we found that the newly measured mass of ^{100}Sn was responsible for the poorer fit. However, there is a large error bar on that measurement. If one is more conservative and includes only data that has a experimental error of less that 200 keV, the minimax is only increased slightly. The main lesson from this analysis is that one can prioritize the importance of accurate mass measurements of individual nuclei, and ^{100}Sn certainly deserves further study.

The chart of nuclei showing the critical ones is given in Fig. 9. The critical nuclei for

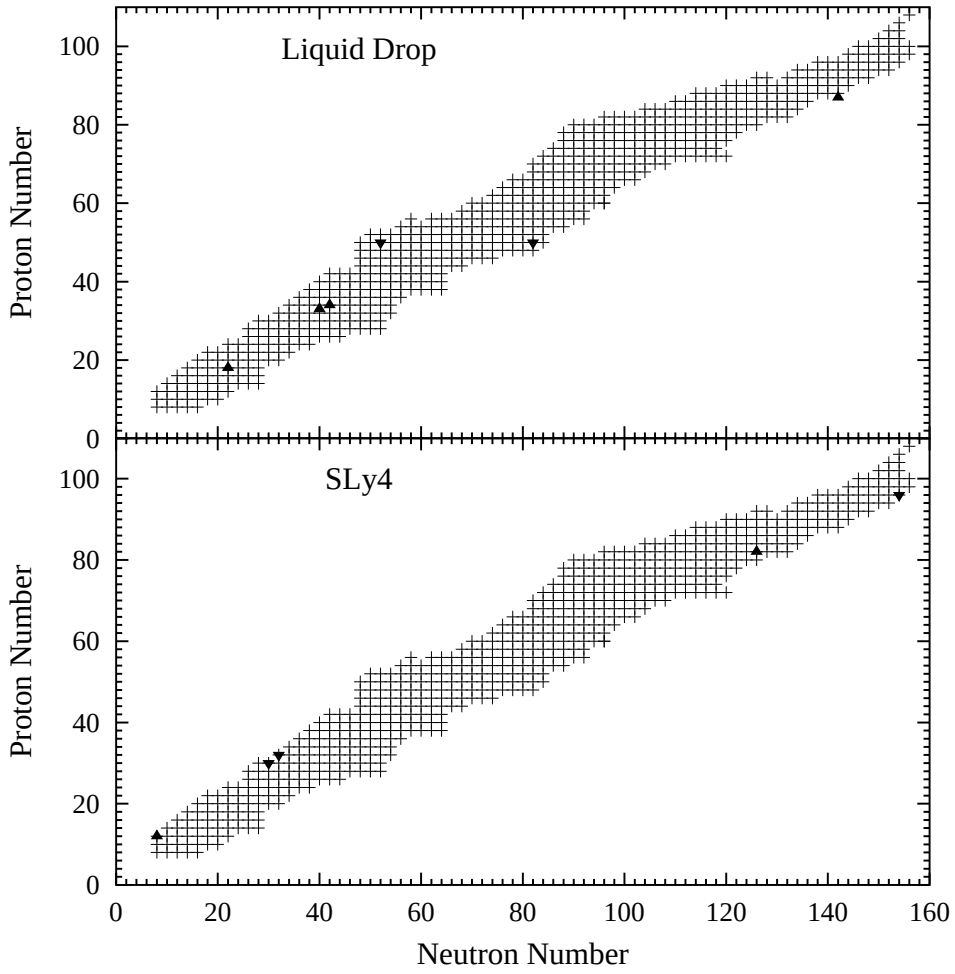

FIG. 9: Chart of nuclei showing the critical nuclei of the liquid drop model and of the linearized refit of the SCMF based on the SLy4 interaction. Critical nuclei are indicated by triangles, with the orientation of the triangle distinguishing overbound (Δ) and underbound (∇) nuclei. The cross area shows the nuclei whose masses have been measured.

TABLE VII: Liquid drop model, comparing least squares fits with minimax fits of the 2003 and 1995 mass tables [17]. The fit does not include light nuclei (N or $Z < 8$).

Data set	r.m.s. (MeV)	C-norm (MeV)	overbound critical nuclei underbound critical nuclei
2003	2.9	9.2	^{40}Ar, ^{76}Se,^{77}Br,^{229}Fr ^{100}Sn,^{132}Sn
1995	3.0	8.0	^{73}Ge,^{101}Nb,^{230}Ra ^{23}O,^{132}Sn,^{207}Pb
2003 $\sigma < 0.2$ Mev	2.8	8.4	^{40}Ar,^{73}As,^{76}Se,^{229}Fr ^{102}Sn,^{132}Sn

the SCMF/Sly4 include the doubly magic ^{208}Pb, a very heavy neutron-rich nucleus, and two nuclei on the $N = Z$ line. We already saw in Sect. IV D that the SCMF does not properly decribed the enhanced binding of the alpha-particle nuclei.

G. Energy landscapes, intruder states, and fission barriers

In this section we will going beyond the minimum point of the SCMF. The purpose ultimately is to get information about excitations, to assess the reliability of the computed minimum, and to make a better theory of the ground state. To get away from the minimum, simply add an external potential to the Hamiltonian and recalculate the SCMF ground state. Quadrupole deformations can thus be artificially induced by adding a quadrupole field, e.g.

$$H \to H - \lambda Q.$$

Here λ is an arbitrary parameter that can be adjust to achieve a desired degree of deformation. In practice, `ev8` allows you to specify the deformation you want in the input file. The code has an iterative procedure to choose the λ appropriately. I will now show some examples that were obtained with the SLy4 parameters in a Skyrme energy functional. The first example is ^{28}Si, a nucleus that should be magic in a spin-orbit dominated shell model. The energy landscape is shown in Fig. 10. In calculating the energies, one takes the expectation value of the Hamiltonian (or evaluated the energy functional) omitting the external field but taking the wave function from the calculation that included the field. One sees that the

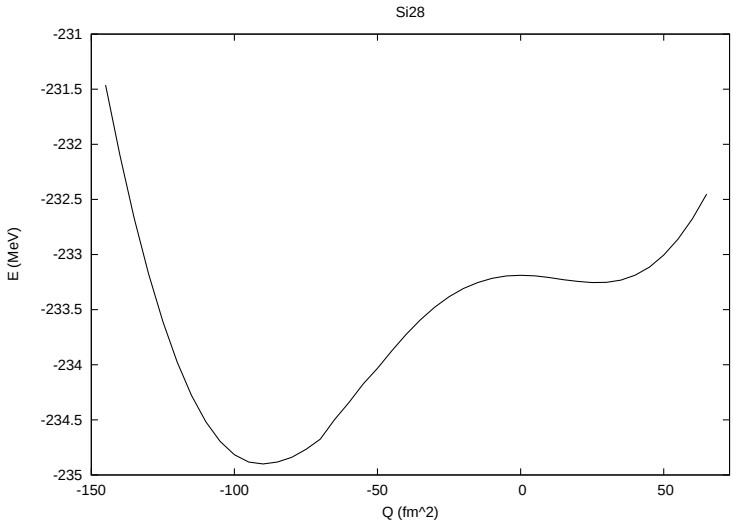

FIG. 10: Potential energy landscape for ^{28}Si.

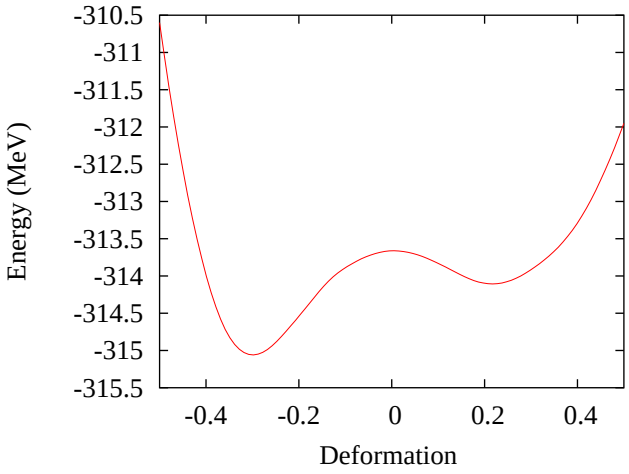

FIG. 11: Potential energy landscape for ^{42}Si.

minimum is not a spherical state but is rather an oblate deformed state. The difference in energy is rather small (1.8 MeV) suggesting that the shape may not be so rigidly determined. The next example is ^{42}Si which is the subject of a very recent article in *Nature*, where it was asserted to be doubly magic [11]. The energy landscape is shown in Fig. 11. So theory predicts that the nucleus should be oblate. What do you think?

When the energy landscape has a minimum brought about by a major rearrangement of the orbitals, the state that is generated is called an *intruder state*. It is not a part of the space of the normal shell orbitals for that nucleus, but it intrudes into it from higher shells. A famous example is the nucleus ^{16}O. According to the naive shell model, its low excited

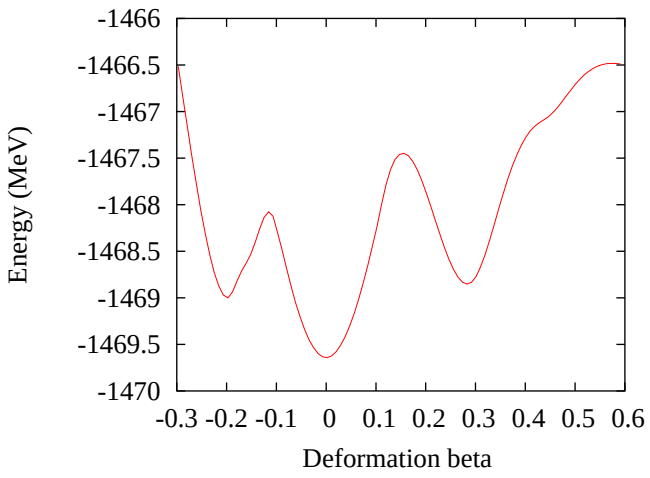

FIG. 12: Potential energy landscape for ^{188}Pb.

states should come from particle-hole configurations with the particle in the *sd*-shell and the hole in the *p*-shell. This implies that the states would all have odd parity. In fact the lowest excited state has 0^+ quantum numbers, and has a highly deformed intrinsic structure. There is no hint of a flat landscape allowing a second 0^+, but we will see that extensions of the SCMF bring down a highly deformed state.

The next example is ^{188}Pb, from ref. [20]. This gives a much clearer example of coexistences of states of different character in the same part of the spectrum. Besides having a 0^+ ground state, its first two excited states also have 0^+ quantum numbers. Its energy curve is shown in Fig. 12. One sees three minima: oblate, spherical, and prolate. We will see later how to extend the SCMF to get an actual spectrum of excited states. spectrum.

The energy landscape is also of interest in describing fission. There is a complex set of phenomena associated with the fission process in plutonium. First of all, there is the barrier, the lowest energy that fission can take place without tunneling. In addition, there are multiple minima along the route to fission, that affect the strength function. A computed fission barrier is shown in Fig. 13. The ground state is the lowest point on the curve located near $Q = 70$ bn. The second well, labeled E_{II}, is responsible for fission isomers. The actual fission barrier is located at the point E_B. When the energy of the nucleus just exceeds the barrier, in mainly decays by fission.

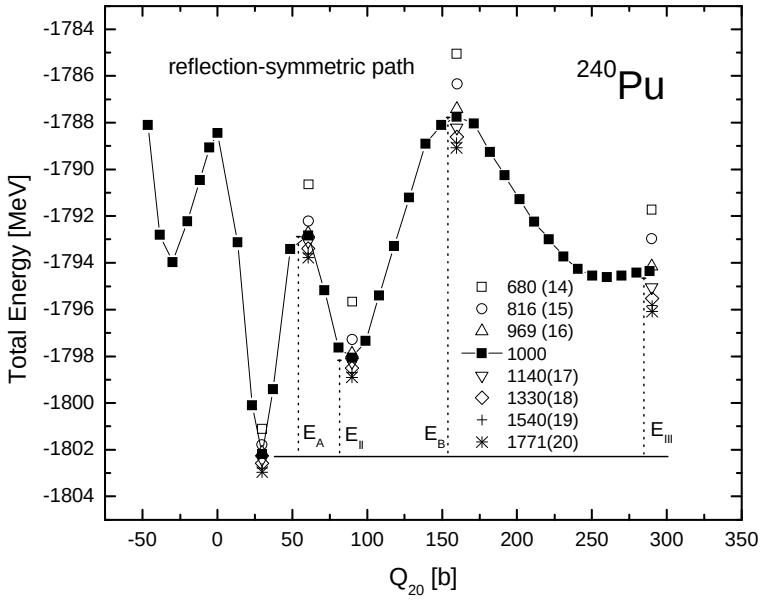

FIG. 13: Fission barrier in ^{240}Pu, calculated in the SCMF with the Skyrme SLy4 functional.

PART II: BEYOND THE SCMF

There are two main approaches to improve on the SCMF. One approach fixes the problem that the wave function often does not conserve the symmetries of the Hamiltonian, particularly rotational invariance for deformed nuclei and particle number for nuclei with BCS condensates. The remedy is to project the SCMF wave function onto eigenstates of the quantum number in question. The other approach is a more general one; one introduces other states (configurations) into the theory and mixes them together. Conceptually this is straightforward. However, the computational obstacles are enormous and simplified approximation schemes play an important role.

V. PROJECTIONS

We begin with particle number projection. One often uses the formula,

$$\hat{P}_N = \frac{1}{2\pi}\int_0^{2\pi} d\phi e^{i(N-\hat{N})\phi}$$

to project a good particle number from a BCS wave function or from a grand canonical density matrix. For example, we would project out particle number N from a BCS wave

function using the matrix elements

$$\langle BCS|e^{i\hat{(N)}\phi}|BCS\rangle = \prod_i^{N_{orb}} (u_i^2 + e^{2i\phi} v_i^2)$$

The projected overlap is then given by the Fourier transform integral,

$$< BCS|\hat{P}_N BCS >= \frac{1}{2\pi} \int e^{-N\phi} \prod_i^{N_{orb}} (u_i^2 + e^{2i\phi} v_i^2) d\phi$$

which is usually carried out numerically. Since the maximum frequency in the exponential is $2N_{orb}$, the integral can be done exactly using a uniform mesh with $2N_{orb}$ integration points.

Next we look at the corresponding projection formula for angular momentum. A deformed intrinsic state having angular momentum K about the z-axis con be projected onto angular momentum J, M by the operator

$$\hat{P}_{JMK} = \frac{1}{8\pi^2} \int d^3\Omega \mathcal{D}^J_{MK}(\Omega) \hat{R}_\Omega.$$

Here $\hat{R}_\Omega$ is the operator that rotates the wave function through Euler angles $\Omega = (\alpha, \theta, \gamma)$, $d^3\Omega = d\alpha\, d\cos(\theta)\, d\gamma$ and $\mathcal{D}^J_{MK}$ is the Wigner function. In general, the numerical evaluation of the three-dimensional integral needs too many integration points to be practical. Fortunately, for some wave functions, namely those that are axially symmetric, the integration reduces to one dimensional. In that case we obtain the J-state with $M = 0$ using the operator

$$\hat{P}_J = \frac{1}{2} \int_{-1}^{1} d\cos\theta P_J(\cos\theta) \hat{R}_y(\theta) \tag{4}$$

where $\hat{R}_y(\theta)$ rotates the wave function by an angle θ about the y-axis and $P_J(x)$ is the Legendre function.

The computer program `promesse`, available on request from its authors [23], carries out particle number projection and calculates the matrix elements needed for angular momentum projection, taking as input the file of SCMF orbitals generated by `ev8`. It automatically takes enough integration points in the gauge angle to do the exact number projection, but selection of rotation angles for the angular projection often needs to be made by the user. It takes much longer to do the projections than to calculate the SCMF orbitals. The angular projection is carried out by making a polynomial fit to the wave function on the Cartesian mesh and using that approximation to interpolate the orbital functions on a rotated mesh. To accurately rotate the N_x^2 points in a given plane takes of order N_x^4 operations, which is a significant computational cost [43].

Having established that projection can be carried out, let's ask the most important practical question about it: does it make a better theory? There is a spectroscopic side and an energetics side to the question. No one has given a convincing answer to the question for particle projection, but the utility of angular momentum projection is clear. In a study of correlation energies for the known-mass even-even nuclei, our group found that a better fit to the energies could be made including a separation term for the rotational projection[5]

VI. RPA AND QRPA

A very useful extension of SCMF is the RPA theory of the excitation spectrum. RPA can be derived in many ways, and I have gone through a number of these derivations in lectures I have given in the past [15]. A good way to view it is as a small-amplitude approximation to time-dependent SCMF, which in turn can be derived from the variational principle

$$\delta \int dt \, \langle \Psi(t) | H - i \frac{\partial}{\partial t} | \Psi(t) \rangle,$$

where the varied wave function $|\Psi(t)\rangle$ is restricted to be of determinantal form. This is the case if we can write $|\Psi(t)\rangle$ in the form $|\Psi(t)\rangle = exp(iW(t))|\Psi_0\rangle$ where $W(t)$ is a Hermitian one-body operator and $|\Psi_0\rangle$ is the SCMF ground state. In its most general form, the RPA theory take $W(t)$ to be

$$W(t) = \sum_{ph} (\sin \omega t \, Y_{ph} + i \cos \omega t \, X_{ph}) a_p^\dagger a_h) + \text{c.c.}$$

Here X_{ph}, Y_{ph} are vectors in the space of particle-hole configurations; the equation they satisfy is

$$\begin{bmatrix} A & B \\ -B & -A \end{bmatrix} \begin{pmatrix} Y \\ X \end{pmatrix} = \omega \begin{pmatrix} Y \\ X \end{pmatrix} \tag{5}$$

where A and B are Hamiltonian matrices in the particle-hole space. Thus, if the space has N_h occupied orbitals and N_p unoccupied orbitals there will be $2N_nN_p$ real amplitudes to describe the wave function. Although the dimension of the matrix is $2N_nN_p$, there are only N_nN_p distinct excitations, corresponding in number to the number of particle-hole configurations. The RPA has the important property that it respects conservation laws embedded in the Hamiltonian, most particularly the relation between current and density. This is exhibited in energy-weight sum rules, and gives the RPA its prominence in the theory of giant resonances.

TABLE VIII: Excitation energy of the first 2^+ in ^{48}Ca, in MeV

Source	Excitation energy
i.p.	4.3
RPA	3.6 [33]
exp.	3.8

For an example of an RPA calculation, I return to the first excited state in ^{48}Ca where we saw the failure of the independent particle model. Including interaction effects, the energy of the particle-hole state will be lowered, bringing it closer to experiment. Ref. [33] reports some RPA calculations for this nucleus. For the energy functionals closest to the one we use, they a value of 3.8 MeV for the excitation energy.

The quasiparticle RPA (QRPA) is the generalization to systems with HFB or HF-BCS ground states. The equations are similar, replacing particle-hole amplitudes by two-quasiparticle amplitudes. In HFB, all orbitals are (in principle) occupied, so the dimension of the space becomes the square of the orbital space dimension. This can be very large for the lattice representation of orbitals. For an example of the application of QRPA , ref. [34] calculates excitations in neutron-rich *sd*-shell nuclei using it. They find that the excitation energy of the lowest 2^+ excitation is lowered by the interaction effects. One of the currently interesting applications of the QRPA is to beta decay strength functions in heavy nuclei [36]. Here the particle-hole operator changes a neutron into a proton or vice versa. The QRPA was first applied in this context by a student of mine [12].

VII. GENERATOR COORDINATE METHOD

We now describe how to get spectra from the energy landscapes we computed in Sec. IV G. There is a systematic procedure for doing this with any kind of field called the Generator Coordinate Method (GCM). The strength of the field, e.g. ω or λ, is a variable used to "generate" a set of configurations, and then the expectation of the Hamiltonian is minimize in that configuration space. Formally the generating parameter is treated as a continuous variable, but for actual calculations it is taken with discrete values and we shall treat it that way here.

The logic of the method is quite straightforward. Let us label the constrained configurations in some way, perhaps by the expectation value of the constraining operator. Thus we call the state $|q\rangle$ that is generated by solving the SCMF in the presence of the external field λQ setting $q = \langle Q \rangle$. The ground state energy is calculated by minimizing the expression

$$E = \frac{\langle \Psi | H | \Psi \rangle}{\langle \Psi | \Psi \rangle} \tag{6}$$

where $|\Psi\rangle = \sum_i c_i |q_i\rangle$ and the c_i are variational parameters. Carrying out the variation, one obtained the Hill-Wheeler equation to be satisfied by the solution. In discrete form, it is the matrix equation,

$$\sum_j (\langle q_i | H | q_j \rangle - E \langle q_i | q_j \rangle) c_j = 0$$

The stumbling point for using the formula is the typical overcompleteness of the space of states. When that happens, the matrix equation is unstable and one can spurious solutions. This can be dealt with by the same trick we used for the fitting problem when there were too many parameters. As an examples of the use of this method I show the energy landscapes and computed spectra for the nuclei ^{16}O [40] and ^{186}Pb [41]. See Figs. 14 and 15. The GCM does remarkably well for the excited state spectrum of ^{16}O. The energies are very good compared to the results of the configuration-mixed shell model. Also, the low transition rates come out within a factor of two of the experimental values. The theory for ^{186}Pb also predicts that the first excited state has spin zero, in agreement with experiment. Both these nuclei exhibit the coexistence phenomenon, namely the presence of a deformed band in the same part of the spectrum as the ordinary states.

The GCM is also used in a quite different way, to derive collective Hamiltonians. This is carried out by making the Gaussian overlap approximation (GOA):

$$\langle q | q' \rangle \approx \exp(-\alpha (q - q')^2);$$

$$\langle q | H | q' \rangle \approx \langle q | q' \rangle (h_0 - (q - q')^2 h_2).$$

Here $\alpha,\ h_0,\ h_2$ are functions of $\bar{q} = (q + q')/2$. Those functions are then used to construct a collective Hamiltonian. One can see how this works by taking q to be continuous coordinate, and $\alpha, h_0, and h_2$ to be constant. Then the equation can be solved by plane waves,

$$\int dq \, (\langle q' | H | q \rangle - E \langle q' | q \rangle) e^{ipq} = 0.$$

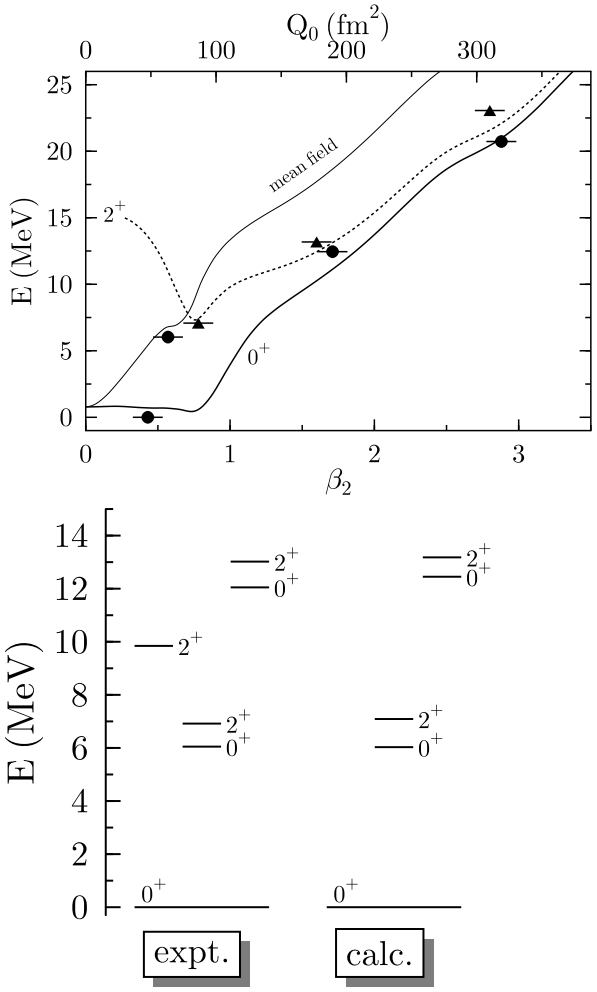

FIG. 14: Energy landscape of ^{16}O with superimposed spectrum from the GCM theory, Figs. 3 and 4 from [40].

FIG. 15: Energy landscape of ^{186}Pb with superimposed spectrum from the GCM theory, Figs. 1 and 4 from [42].

Evaluating the integrals gives

$$(h_0 - h_2\frac{p^2}{4\alpha} - E)e^{ipq'}e^{-p^2/4\alpha} = 0??$$

Thus, we can identify h_0 with the potential energy in a collective Hamiltonian and $h_2/4\alpha$ with the coefficient $1/2M$ in a kinetic term $p^2/2M$. This method has been applied to the quadrupole coordinate to construct a collective Bohr Hamiltonian, which was then solved to get spectroscopic properties [45]. One can also make a connection between the GCM/GOA and the RPA, if one replaces the constant $h - 0$ by a quadratic function of q. For details of

the algebra, see [47].

Even when the discrete form of the GCM is kept, the GOA can be useful. Let us first return to the angular momentum projection, which we do by performing the integral eq. 4 numerically. When we did our global study of correlation energies, it was very important to do the integral efficiently. It turned out that the GOA permits one to compute the integrals just using a 2-point evaluation of the overlaps. But instead of using θ or $\cos\theta$ as a variable, it better to use $\sin\theta$, i.e

$$\langle q|\hat{R}_\theta|q\rangle \approx e^{-c\sin^2\theta}.$$

The reason is that the wavefunction is invariant under rotations by an angle π, and the GOA should respect it. This is called the topological Gaussian overlap approximation (top-GOA) [48].

The GOA is also useful for computing the overlaps between different deformations q_i. Here one orders the states and uses the computed overlap between neighboring configurations to determine a distance scale x, $\langle q_i|q_{i+1}\rangle = e^{-(x_i-x_{i+1})^2/2}$. Then any other overlap is estimated from the assigned x scale, $\langle q_i|q_j\rangle = e^{-(x_i-x_j)^2/2}$. These two GOA's reduce the computation task of the discrete Hill-Wheeler by two orders of magnitudes in a typical situation where there are about ten configurations to be included in the Hill-Wheeler equations [21].

Simplifying the GCM in this way, Bender, Heenen and I have computed the correlation energies of the known even-even nuclei. Adding the correlation energy to energy from the SCMF, we found that there was some improvement in the binding energy. The improvement is most noticible in the differential quantities, namely the separation energy and the two-nucleon gap. In the graph of the two-proton gaps systematics for Sn and Pb, Fig. VI, the solid line shows the theory including the quadrupolar correlation energy. One sees quit a good agreement with the experimental values.

VIII. AUXILIARY FIELD METHODS

The auxiliary field method is a powerful technique that in effect reduces a two-particle Hamiltonian to a form that only has one-particles fields. It is used in many areas of physics, particularly condensed matter, and it is closely related to the path integral method of quantum field theory. It also is interesting from a formal point of view because SCMF and extensions of SCMF such as RPA can be easily derived from it. To discuss it, we need to

distinguish between operators that act in the many-particle Fock from those that are simple matrices in a one-particle space. Let us use carats for Fock-space operators such as the particle creation and annihilation operators, which we now write as $\hat{a}^\dagger, \hat{a}$. The basic object of study in the auxiliary field method is the many-particle imaginary-time evolution operator $\exp(-\beta\hat{H})$. Its trace (Tr_F in many-particle Fock space) is the grand canonical partition function, if $\hat{H}$ is replaced by $\hat{H} - \mu N$. The basic formula is for the expectation value of an operator $\hat{K}$ in the grand canonical ensemble at inverse temperature β is:

$$\langle\hat{K}\rangle = \frac{\mathrm{Tr}_F\, \hat{K} e^{-\beta\hat{H}}}{\mathrm{Tr}_F e^{-\beta\hat{H}}}. \tag{7}$$

The first step to get a practical calculational method is to slice it into factors that can be approximated more easily:

$$\exp(-\beta\hat{H}) = \prod^{N_t} \exp(-\Delta\beta\hat{H})$$

where $\Delta\beta = \beta/N_t$, and N_t is the number of terms (called "time slices"). This is called the Trotter expansion. Next, assuming $\Delta\beta$ to be small, an individual term can be separated into kinetic and potential parts as

$$e^{-\Delta\beta\hat{H}} \approx e^{-\Delta\beta\hat{t}} e^{-\Delta\beta\hat{v}}$$

where $\hat{v}$ is a two-particle potential energy. The next step is the Hubbard-Stratonovich transformation, which carries us from the two-particle operator $\hat{v}$ to an expression containing only one-particle operators. First it is necessary to express the interaction as a sum over products of one-particle operators,

$$\hat{v} = -\frac{1}{2}\sum_i^{N_O} \hat{O}^i \hat{O}^i$$

Here the one-particle operators $\hat{O}$ have the form $\hat{O} = \sum_{ik} \mathrm{O}_{ik} a_i^\dagger a_k$. The number of terms in this separable expansion is N_O. For a single term, the Hubbard-Stratonovich transformation is the identity

$$e^{-\Delta\beta\hat{H}} = \sqrt{\frac{\Delta\beta}{2\pi}} \int_{-\infty}^{\infty} d\sigma_i e^{-\Delta\beta\hat{h}} e^{-\Delta\beta\sigma_i^2/2}$$

where the single-particle Hamiltonian $\hat{h}$ is given by

$$\hat{h} = \hat{t} + \sigma_i \hat{O}_i$$

Using it, the Trotter expansion becomes a many-dimensional integral over the exponentiated one-particle Hamiltonians $\hat{h}$. This is often written

$$\int \mathcal{D}[\sigma]\, e^{-\int d\beta\, \sigma^2/2} e^{-\int d\beta\, \hat{h}(\sigma)} \tag{8}$$

where $\mathcal{D}[\sigma]$ represents the many-fold integrations over the σ fields. The dimension of the integration is $N_t N_O$. Note that the interaction must be attractive for this formula to work. Fortunately for nuclear physics the most important parts of the interaction for nuclear structure purposes are attractive.

Before mentioning the interesting applications of the formula, I will show you how easy it is to derive the mean-field approximation. Let's look at the denominator in the trace formula, which we now write

$$\int \mathcal{D}[\sigma]\, e^{-\int d\beta \sigma^2/2} \mathrm{Tr}_F\, e^{-\int d\beta\, \hat{h}(\sigma)}.$$

The simplest possible approximation to this integral is to replace the integrand by a single point. Obviously, if we do that, we should choose the point the integrand is a maximum. Thus, we now evaluate the simplified trace having all the σ's equal,

$$\mathrm{Tr}_F\, e^{-\beta(\hat{t}+\sigma\hat{O})}.$$

To evaluate the trace, we diagonalize the single-particle Hamiltonian to get eigenenergies $\epsilon_i(\sigma)$. Then the trace becomes

$$\mathrm{Tr}_F\, \exp(-\beta \sum_i \epsilon_i \hat{n}_i) = \prod_i (1 + e^{-\beta\epsilon_i}).$$

Up to now I have ignored the chemical potential, but it can't be avoided any longer. Let us suppose we want to treat N particles. Then the chemical potential should be chosen so that N of the eigenvalues ϵ_i are negative. If β is large, the product can then be approximated as

$$exp(\beta \sum_i^N \epsilon_i).$$

Next we determine σ to maximize the complete integrand, $\exp(-\beta\sigma^2/2 + \beta \sum_i^N \epsilon_i)$. Setting the derivative to zero, the condition is

$$\sigma = \sum_i^N \frac{d\epsilon(\sigma)}{d\sigma}.$$

But, remembering the Feynman-Hellman theorem, this may be seen equivalent to Hartree self-consistency condition $\sigma = \langle \Phi_{HF} | \hat{O} | \Phi_{HF} \rangle$.

It is also possible to derive a formula for the RPA correlation energy from the trace formula [25].

A. Thermal properties

Eq. 7 is very useful for treating the thermal properties of nuclei, as it is just the grand canonical expectation value for the operator $\hat{K}$ at temperature $T = 1/\beta$. To apply this to the nuclear level density, one first calculates the expectation value of the Hamiltonian as a function of β,

$$E(\beta) = \frac{\mathrm{Tr}_F \, \hat{H} e^{-\beta \hat{H}}}{\mathrm{Tr}_F e^{-\beta \hat{H}}}.$$

The partition function $Z(\beta)$ may then be computed by integrating the energy function,

$$Z(\beta) = Z(0) exp(- \int_0^\beta d\beta' \, E(\beta').$$

The level density can be obtained from the partition function by using the saddle point approximation. That yields

$$\rho_\beta = \frac{1}{\sqrt{2\pi C}} Z(\beta) e^{\beta E_\beta}.$$

It is straightforward to derive the finite-temperature HF theory from the single-point approximation to the integral, as was done with the ground state theory (large β).

Another approximation I want to mention briefly is the *static path* approximation, defined by keeping σ independent of time slice (thus static), but keeping the full integral over the values of σ. It has been used to discuss the effect of projections and symmetry breaking on the nuclear level density. The theory of level densities derived from the independent orbital approximation has a different prefactor, depending on whether the nucleus is spherical or deformed [18]. The static path approximation gives a way to treat both cases as well as the soft nuclei in between [30]. More recently, Alhassid and I used it to generalize the Belyaev formula for moments of inertia to finite temperature and to take into account differences between odd and even nuclei [44]

B. SMMC and MCSM

The so-called Shell Model Monte Carlo makes use of a stochastic evaluation of the integrals in the auxiliary field formula. When the number of integration variables is larger than six or so, it becomes impractical to use meshes for their evaluation. On the other hand, using importance sampling the ratio of integrals

$$\frac{\int \mathcal{D}[\sigma] A(\sigma) P(\sigma)}{\int \mathcal{D}[\sigma] P(\sigma)}$$

can be estimated to acceptable accuracy. Here $P(\sigma)$ is the integrand which must be nonnegative for the method to work. The importance sampling technique is to produce an ensemble of points σ^k (actually vectors of dimension $N_t N_O$) whose density in the integration space equal to the integrand in the denominator. With that ensemble the estimator of the ratio of integrals is

$$\frac{1}{N} \sum_k^N A(\sigma^k)$$

The ensemble of points is generated by the Metropolis algorithm, which I will not go through in detail. The art of using the algorithm is in defining how a candidate for the next point is generated from the previous point using the probability function $P(\sigma)$. I will explain now how $P(\sigma)$ is computed. The crucial point is that the evolution operator $\hat{U}(\sigma) = \prod_i \exp(-\Delta\beta(\hat{t} + \sigma_i \hat{O})$ is a one-body operator that can be diagonalized in the one-body space for use in the Fock space. In the one-body space the matrix is $U = \prod_i \exp(-\Delta\beta(t + \sigma_i O))$; diagonalizing it gives a set of eigenvectors ξ_k and eigenvalues λ_k. Then the full many-particle operator $\hat{U}$ can be expressed

$$\hat{U} = \prod_k (1 + \lambda \sum_{ij} \xi_{ki} \xi_{kj} \hat{a}_i^\dagger \hat{a}_j).$$

For example, we can use this to evaluate the Fock-space trace

$$\mathrm{Tr}_F \hat{U} = \prod_k (1 + \lambda_k)$$

and the trace of a single-particle operator with $\hat{U}$,

$$\mathrm{Tr}_F \hat{O}\hat{U} = \sum_k \frac{(1 + \lambda_k \langle k|O|k\rangle)}{(1 + \lambda_k)} \mathrm{Tr}_F \hat{U}.$$

The formulas are only slightly more complicated for traces of products of single-particle operators, needed for evaluating the two-body Hamiltonian.

Thus, we can find the many-particle quantities dealing only with matrices in the single-particle space. This gives the SMMC excellent scaling properties with respect to the size of the nucleus. Here is a naive analysis of the numerics: Call the number of time slices M_t, and the dimension of the single-particle space N_ϕ. The matrix multiplications to compose U each take N_ϕ^3 operations, and that has to be done M_t times. The diagonalization is also N_ϕ^3, which is hardly noticeable after the multiplications. Thus the scale of the effort is

$$N_\phi^3 M_t.$$

This may seem like a lot, but it is small compared to the effort needed to treat explicitly the many-particle configurations by matrix methods. The dimensions here grow exponentially with the number of particles in the system.

Up to now, this method has only been applied using the spherical shell model to construct the single-particle basis. But there is no reason that one couldn't use the SCMF orbitals as a more efficient basis.

Finally, I want to mention the MCSM which has been developed by Otsuka and collaborators [35]. In some way his approach is intermediate to the GCM and the auxiliary fields. As in the SMMC, one constructs configurations using the Trotter expansion $|\sigma\rangle = e^{\int d\beta\, \sigma O}|\Psi_0\rangle$. However, one doesn't try to integrate over all σ fields but rather uses the configurations as a basis. Thus, the equation to be solved in the end is the same variational equation as eq. 6.

Acknowledgments

The author acknowledges support by the US Dept. of Energy under Grant FG02-00ER41132.

---

[1] M. Bender, P.-H. Heenen, P.-G. Reinhard, Rev. Mod. Phys. **75**, 121 (2003).

[2] P. Ring, P. Schuck, *The Nuclear Many-Body Problem*, Springer Verlag, New York, Heidelberg, Berlin, 126,314,438 (1980).

[3] J. Bardeen, L. N. Cooper, and J.R. Schrieffer. Phys. Rev. **108** (1957).

[4] P. Bonche, H. Flocard, P.-H. Heenen, Computer Phys. Comm. **171** 49 (2005).

[5] M. Bender, G.F. Bertsch, P.-H. Heenen, Phys. Rev. Lett. 94 (2005) 102503.

[6] M.V. Stoitsov, J. Dobaczewski, W. Nazarewicz, and P. Ring, Computer Phys. Comm. **167** 43 (2005).

[7] G.A. Lalazissis, S. Raman and P. Ring, ADNDT **71** 1 (1999).

[8] M. Kleban, et al., Phys. Rev. C 65, 024309 (2002).

[9] H. Flocard, et al., Phys. Rev. **C17** 1682 (1978).

[10] E. Chabanat, P. Bonche, P. Haensel, J. Meyer, and R. Schaeffer, Nucl. Phys. **A635**, 231 (1998), Nucl. Phys. **A643**, 441(E) (1998).

[11] J. Fridmann, et al., Nature **435** 922 (2005).

[12] D. Cha, Phys. Rev. **C27** 2269 (1983).

[13] P. Möller, J. R. Nix, W. D. Myers, and W. J. Swiatecki, Atom. Data Nucl. Data Tables **59**, 185 (1995).

[14] G. F. Bertsch, B. Sabbey, M. Uusnäcki, Phys. Rev. C **71**, 054311 (2005).

[15] G.F. Bertsch, in Les Houches, Session LXVII, 1996, p. 123; Les Houches, Session LXXIII, 2001, p. 57; *Introduction to modern methods of quantum many-body theory and their applications*, (World Scientific, 2002), p. 1; also available at the web site `http://gene.phys.washington.edu/~bertsch/pedlist.html`

[16] `http://gene.phys.washington.edu/~bertsch/computer.html`

[17] G. Audi, A. H. Wapstra, and C. Thibault, Nucl. Phys. **A729**, 337 (2003); the data file is available at `http://www-csnsm.in2p3.fr/AMDC/masstables/Ame2003/mass.mas03`.

[18] A. Bohr and B.R. Mottelson, *Nuclear Structure*, Vol. II (Benjamin, 1975).

[19] F. Tondeur, S. Goriely, J. M. Pearson, M. Onsi, Phys. Rev. **62**, 024308 (2000).

[20] M. Bender, et al., Phys. Rev. **C69** 064303 (2004).

[21] M. Bender, G.F. Bertsch, and P.-H. Heenen, Phys. Rev. C**69** 034340 (2004).

[22] S. Raman, et al., ADNDT **78** 1 (2001).

[23] M. Bender, P. Bonche, and P.-H. Heenen, unpublished.

[24] S.E. Koonin, D.J. Dean, and K. Langanke, Phys. Rep. **278** 2 (1997).

[25] A.K. Kerman, S. Levit, Phys. Rev. C **24** 436 (1981).

[26] A. Staszczak, J. Dobaczewski, and W. Nazarewicz, Int. J. Mod. Phys. E **14** 395 (2005).

[27] S. Cwiok, P.H. Heenen, and W. Nazarewicz, Nature **433** 705 (2005).

[28] S.M. Fischer, et al., Phys. Rev. Lett. **87** 132501 (2001).

[29] Y. Utsumo, T. Otsuka, T. Mizusaki, and M. Honma, Phys. Rev. C **60** 054315 (1999).

[30] B. Lauritzen and G.F. Bertsch, Phys. Rev. C **39** 2412 (1989).

[31] W. Kohn and L. Sham, Phys Rev. **A137** 1697 (1965).

[32] R.P. Feynman, Phys. Rev. **56** 340 (1949); H. Hellmann, Einfuehrung in die Quantenchemie (Deuticke, Leipzig, 1937).

[33] I. Hamamoto, H. Sagawa, and X.Z. Zhang, Nucl. Phys. A **626** 669 (1997).

[34] M. Yamagami and N. Van Giai, Phys. Rev. C **69** 034301 (2004).

[35] T. Otsuka, T. Mizusaki, and M. Honma, J. Phys. G **25** 699 (1999)

[36] J. Engel, et al., Phys. Rev. C **60** 014302 (1999).

[37] D.R. Hartree, Proc. Cambridge Phil. Soc. **24** 111 (1928); V. Fock, Z. Physik **75** 622 (1927).

[38] J.P. Perdew, K. Burke, and M. Ernzerhof, Phys. Rev. Lett. **77** 3865 (1996).

[39] J.P. Perdew, et al., Phys. Rev. Lett. **82** 2544 (1999).

[40] M. Bender and P.-H. Heenen, Nucl. Phys. A **703** 390 (2003).

[41] M. Bender, P. Bonche, T. Duguet, and P.H. Heenen, Phys. Rev. C**69** 064303 (2004).

[42] T. Duguet, M. Bender, P. Bonche, and P.-H. Heenen, Phys. Lett. B **559** 201 (2003).

[43] D. Baye and P.-H. Heenen, J. PHys. A: Math. Gen. **19** 2041 (1986).

[44] Y. Alhassid, et al., nucl-th/0508027 (2005).

[45] J. Libert, M. Girod, and J.-P. Delaroche, Phys. Rev. C **60**, 054301 (1999).

[46] K. Hagino and H. Sagawa, Phys. Rev. C ?? (2005).

[47] `http://gene.phys.washington.edu/ bertsch/rpa.ps`

[48] K. Hagino, G.F. Bertsch, and P.-G. Reinhard, Phys. Rev. C **68** 024306 (2003).